PCCP

Accepted Manuscript

ROYAL SOCIETY OF CHEMISTRY

www.rsc.org/pccp

Manifestation of MOF templated Cu/CuO@TiO$_2$ nanocomposite for synergistic hydrogen production

Indranil Mondal [a,b] and Ujjwal Pal*[a,b]

[a]*Department of Chemistry and Biomimetics, CSIR-Central Mechanical Engineering Research Institute, M.G Avenue, Durgapur-713209, West Bengal, India. E-mail: upal03@gmail.com (Ujjwal Pal), Fax: +91-343-2546745; Tel:+91-343-6452136.*

[b]*Network Institute of Solar Energy, (CSIR-NISE) and Academy of Scientific and Innovative Research (AcSIR).*

Electronic supplementary information available:

Reagent details, FTIR of Cu-BDC and Cu-BDC@Ti(OH)n, TEM and XRD of Cu-BDC particles, pore size distribution curve of photocatalysts, amount of the hydrogen evolved on varying the concentration of Cu and amount of catalyst at optimized condition.

Abstract

Copper Metal-organic framework (Cu-MOF) provides access to Cu/CuO@TiO$_2$ hybrid nanocomposites with highly dispersive copper species adsorbed on TiO$_2$ semiconducting system. This novel nanostructure exhibits efficient hydrogen evolution performance under solar illumination of intensity ~ 1 sun. The rate of the H$_2$ production was systematically optimized under different operational parameters. Experimental observation reveals that mesoporous Cu/CuO@TiO$_2$ nanocomposite with 0.5 wt% Cu loading showed highest rate of H$_2$ production with 286 mmol/g/h, which is fairly higher than that of CuO loaded TiO$_2$, prepared using conventional impregnation method. This high photocatalytic H$_2$ production activity is attributed predominantly to the presence of surface deposited Cu^0 species and the small size heterojunction (1-2 nm) between CuO and TiO$_2$, which synergizes the interfacial charge carrier transfers from TiO$_2$ nanoparticles. The catalyst showed good recyclability under prolonged exposure (30 h) to solar irradiation. Unlike many Pt decorated TiO$_2$ photocatalysts, this hybrid photocatalyst provides an inexpensive means of harnessing solar energy.

Introduction

Owing to useful photophysical properties, metal-oxide nanomaterials are of great interest for the production of solar fuel like hydrogen. In this regard, since pioneering invention made by Fujishima and Honda in 1972.[1] TiO$_2$-based nanocomposites have been widely-studied for H$_2$ production because of low cost, low toxicity, high chemical and thermal stability, and n-type semiconducting nature of host TiO$_2$ counterpart. However, the wide band gap (3.2-3.02 eV) and rapid recombination of photo-generated electron-hole pairs in TiO$_2$, is the biggest obstacle for efficient photocatalytic activity.[2] As the matter of fact, we therefore aim to restrict the charge-carrier recombination process in the bulk semiconductor structure by synthesizing a multicomponent system where MOF-templated synthesis can be a judicious choice to do so. The recombination of photogenerated holes and electrons can be greatly suppressed by fabricating a heterojunction with metal oxide semiconducting materials.[2a,3] Eventually, a marked advancement was accomplished in state-of-the-art regarding the development of TiO$_2$-based nanocomposites with CuO$_x$,[4a] Co$_3$O$_4$,[4b] NiO[4c] etc., but distantly, to understand the effective interracial charge transfer in an active photocatalyst for efficient hydrogen production. In addition a pure metallic cluster attached onto semiconductor surface accelerates the interfacial electron transfer that leads to multi-fold increment of photoactivity. In particular, having high work function, Au and Pt were frequently loaded onto semiconductor surfaces as a co-catalyst for trapping of photogenerated electrons to produce hydrogen.[5] But this is not a cost effective method to employ for large scale application. Standing on this point of view, we therefore believe that this report can be an interesting footstep for development of semiconductor based nanocomposite for clean fuel generation in a cost-effective manner.

Owing to nanoscale pores, size and connectivity of which controlled by combining appropriate metal and linker, metal–organic frameworks (MOFs) can be employed as sacrificial templates, converting into targeted multicomponent nanomaterials as active catalyst.[6] Moreover, pyrolyzing MOFs can effectively reduce their surface area and convert their pores to mesopores while maintaining the open diffusion

channel.[7]   Indeed, proper attachment between MOF and TiO_2 precursor to produce hybrid intermediate and its conversion to nanocomposite by heat treatment is really challenging to us. Despite the great progress achieved so far, the research on the synthesis of inorganic functional materials, especially composite derived from the MOF, is still in its very early stage.

Here we have successfully constructed and characterized MOF-derived $Cu/CuO@TiO_2$ nanocomposite (CMT) photocatalyst where copper species are dispersively adsorbed on the anatase TiO_2 surface.‡ The fabricated nanocomposite showed efficient and synergistic photocatalytic hydrogen generation from water in the presence of sacrificial electron donor (SED) without noble metals. The photocatalyst could be used over a long period of time. This maiden effort to utilize the MOF as template acts as an outstanding candidate in this work, based on their structural properties, robustness and economical synthesis. Titanium isopropoxide $(Ti(ipro)_4)$ and Cu^{2+} are the precursors to make the desired photocatalyst through MOF templated approach. The principal route adopted for this Cu-MOF synthesis is based on mild and facile solvothermal method. The unique synthetic approach led to the formation of CuO and Cu^0 with high dispersion on TiO_2 semiconducting surface.
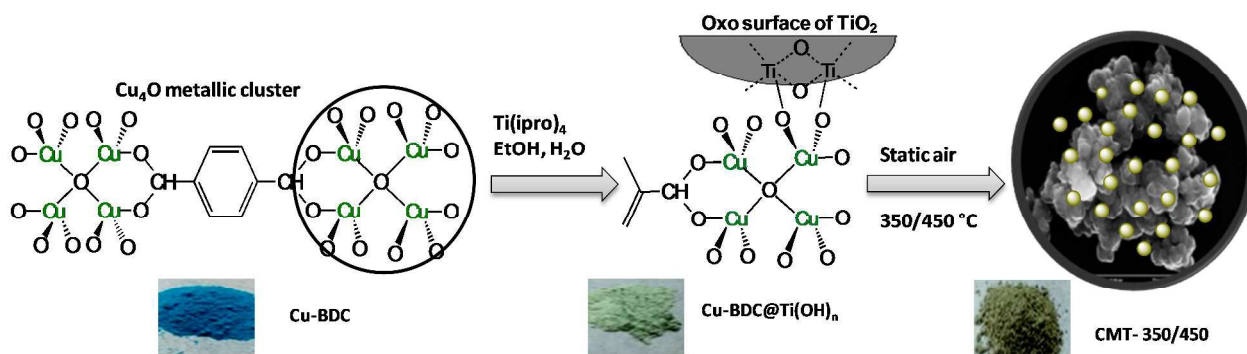
Experimental

Synthesis of [Cu(tpa)·(dmf)] (Cu-BDC)

[Cu(tpa)·(dmf)] (Cu-BDC) was synthesized using some modification of the reported method.[8] In this particular synthetic procedure equimolar quantities of copper nitrate trihydrate (Aldrich, 1.053 g) and terephthalic acid (Aldrich, 0.724 g) were dissolved in minimum amount of N,N'-Dimethylformamide (Merck, DMF) followed by the addition of 20 ml dry methanol. This solution was then placed in a 50 ml autoclave flask and kept in a hydrothermal oven at 95 °C for 36 h. Small blue precipitated crystals were visible inside the flask upon removal from the oven. After repeated centrifugation and washing, the yield was measured to be 80%. Microanalysis demonstrated a close agreement between the synthesized compound and the empirical formula. $C_{11}H_{11}CuNO_5$ (300.76): calcd: C 43.93, H 3.69, N 4.66, O 26.60;

found: C 43.41, H 3.55, N 4.73, O 26.36. Moreover, the as-prepared Cu-BDC was also characterized by

recording its powder XRD pattern (Fig. S3†) which is identical with the reported result.[8]

Synthesis of CMT(x)-350, 450

The adopted methodology was demonstrated schematically in Fig 1. To obtain the final photocatalysts,

calculated amount of Cu-BDC was taken in a round-bottom flask containing 20 ml of 4:1 ethanol/water

mixture, and then it was kept under ultrasonic treatment for 30 min to disperse the particle properly. Then

pre-measured amount of titanium isopropoxide (Ti(ipro)$_4$) was added slowly dropwise with stirring it for

12 h. The resultant green precipitate was recovered by filtration, washed with ethanol and water three

times, and dried in oven at 60 ℃ for overnight. This amorphous material was calcined at 350 and 450 ℃

for 5 h in N$_2$ atmosphere. The final catalysts were designated as CMT(x)-T where x and T define the wt%

of Cu and calcination temperature. The theoretical Cu loading was further checked by ICP analysis for 1

wt% and 3 wt% Cu loaded catalysts and results were tabulated in Table S5†.

Fig. 1 Schematic diagram of MOF-templated synthesis of CMT(x)-T.

Photocatalytic experiment

The photocatalytic H$_2$ generation experiments were carried out in a 100 ml Pyrex glass reactor with flat

optical entry window and external cooling jacket. 20 ml of aqueous suspension containing photocatalysts

(CMT(x)-350 and CMT(x)-450) and 15 v/v% SED were considered as the reaction mixture. Then the

reactor was sealed with rubber septum and sonicated to suspend the catalyst completely in the water/SED

system. Thereafter the photoreactor was deaerated by bubbling argon for 30 min to remove the dissolved

air before light irradiation. It was then stirred and irradiated by 450 W Newport xenon lamp equipped

with AM 1.5G filter. The distance between the lamp and the photoreactor containing reaction solution was fixed at 8 inches. The gaseous products produced were analyzed by Perkin Elmer Clarus GC equipped with 5A molecular sieve column, a thermal conductivity detector and Argon as the carrier gas. The collected data has an error limit of $\pm$ 6%. The durability of the photocatalyst was tested up to 30 h under ambient conditions. The recyclability of the photocatalyst was carried out by opening the sealed reactor, then filtering it, followed by washing in the dark condition and then again loading of the same catalyst under the above mentioned condition before putting it under irradiation. Temperature of the reaction mixture was maintained around 30°C, which as was monitored using temperature controller. Intensity of the light was measured using Newport energy meter (model: 842-PE) which is 100 mW/cm^2 (~ 1 sun).

Physicochemical characterization

Powder X-ray diffraction pattern (PXRD) was performed using a Bruker AXS diffractometer (D8 advance) using Cu-Kα radiation (λ= 1.5406 Å). Sample was scanned in the range of 2θ= 5-100° with the scan rate of 0.5 deg/min and a step size of 0.05 deg. For transmission electronic microscopy (TEM) micrograph, sample was prepared by taking acetone dispersion of the sample on the carbon coated copper grid and drying it at 60 ℃ in static air. These analysis were carried out by JEOL 2010EX operated at an accelerating voltage of 200 kV fitted with a CCD camera. UV-vis diffuse reflectance spectra (UV-vis DRS) was obtained on Labsphere DRA-CA-3300 compartment associated with the Varian Cary 100 spectrophotometer over the 250-800 nm range using $BaSO_4$ as a reference. Field emission scanning electron microscopic (FESEM) images were taken from model LEO, S430i, U.K which was conditioned under 10.00 kV ETH. Brunauer–Emmett–Teller (BET) surface area analysis study was carried out using Quantachrome automated gas sorption data acquisition and reduction instruments version 3.0 under bath temperature 77.35 K. Elemental analyses (C, H, and N) was performed using a 2400 Series-II CHN Analyzer, Perkin Elmer. X-ray photoelectron spectra (XPS) were recorded on a KRATOS AXIS 165 with a dual X-ray anode (Mg and Al); all XPS spectra were recorded using the Mg Kα line. The pressure in the

spectrometer was about 10^{-9} Torr. For energy calibration we have used the carbon 1s photoelectron line at 285.0 eV. Thermo gravimetric analysis (TGA) was carried out using NETZSCH STA 449 F1 Jupiter instrument from ambient temperature to 1000 ℃ in N_2 atmosphere. Linear scan voltammetric (LSV) measurement was carried out on a CH electrochemical workstation CHI600E, in a three electrode cell with a Pt disk counter electrode, a Ag/AgCl reference electrode and a FTO glass coated with photocatalyst as working electrode. All linear seep voltammetric (LSV) measurements were performed in presence of supporting electrolyte of 2M Na_2SO_4. The electrochemical impedance spectroscopy (EIS) measurements were carried out under dark and light condition. 150 W Xe lamp was used as the light source which was fitted with a filter (> 380 nm) and having output illumination intensity of 100 mW/cm^2 The analysis was carried out in the frequency range of 100 kHz to 100 Hz with Ac signal amplitude of 10 mV.

Results and discussion

[Cu(tpa)·(dmf)] (Cu-BDC) was synthesized using some modification of the reported method.[8] The successful attachment between Cu-BDC and TiO_2 hydroxo cluster $(Ti(OH)_n)$ was evidenced by FTIR spectrum of Cu-BDC and Cu-BDC@Ti(OH)$_n$ as shown in Fig. S1†. The characteristic asymmetric (v_a) and symmetric stretching frequency (v_s) for -COO group in Cu-BDC appeared at 1624 cm^{-1} and 1396 cm^{-1} respectively, showed red shift with 49 cm^{-1} and 9 cm^{-1} in the Cu-BDC@Ti(OH)$_n$ composite. This indicates the formation of O-Ti bond between Cu_4O oxo-cluster and Ti. The photocatalyst contains elongated and irregularly shaped nanoparticles were investigated by TEM and FESEM studies. In this regard, CMT(3)-350 catalyst was taken as the representative sample and the morphological information has been depicted in Fig. 2 and 3. TiO_2 nanoparticles with dimension of 30 nm, played as good heterogeneous support for CuO and Cu cluster. Notably, CuO cluster with exposed (111) facets, are closely interconnected with TiO_2 nanoparticles as reflected from the HRTEM analysis (Fig 2c). Eventually this indicates the formation of small size heterojunction, which could play a pivotal role in enhanced hydrogen production. We observed little surface agglomeration in photocatalysts. As shown in

Fig. 2b, tiny Cu nanoparticle (NP's) were visible on TiO$_2$ surface, which again confirmed by

characteristic lattice interplanar distance with 0.21 nm for (111) plane of Cu^0 species.[9] Indeed, Cu-metal-

TiO$_2$ semiconductor Schottky junction is of paramount interest towards charge separation of electron-hole

pairs and storage of electrons in Cu-metal clusters.[10] We believe, more such Schottky junction is likely to

be occurred during the course of photo-irradiation. This further helped to increase the charge separation as

well as charge utilization in photocatalytic process. Fig. S2† showed the TEM image of as-prepared

crystalline Cu-BDC having particle size 25-30 nm.
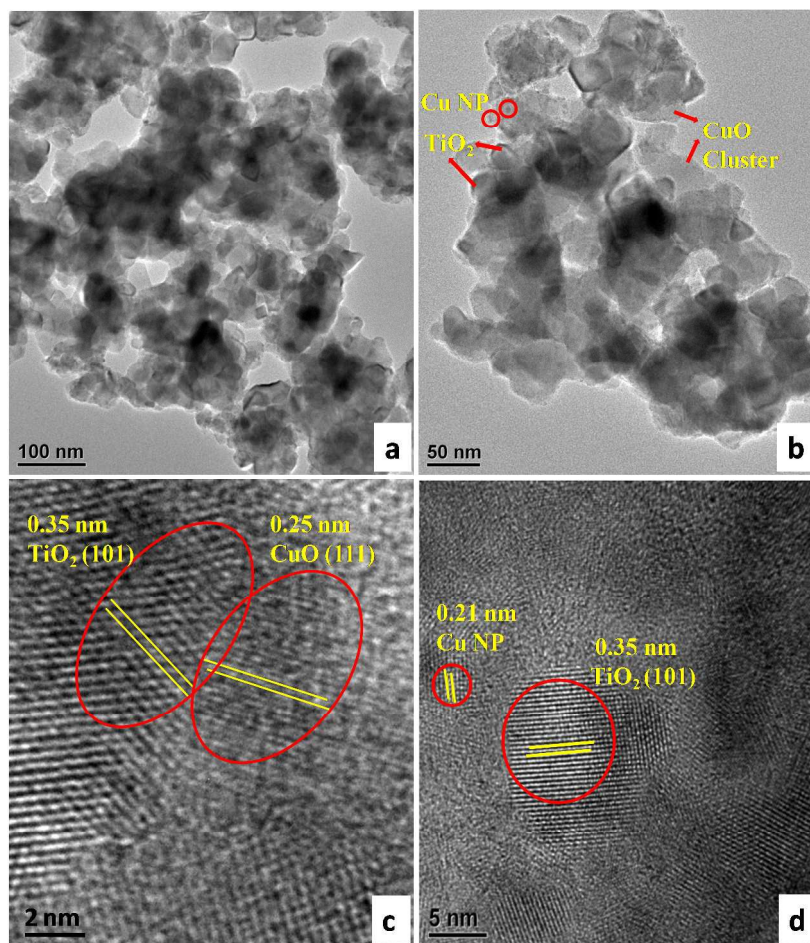
Fig. 2 TEM images of (a) bulk CMT(3)-350, (b) Cu nanoparticle attached on TiO$_2$, (c) lattice fringes for (101) plane of anatase TiO$_2$ and (111) plane of CuO and (d) lattice fringes for anatase TiO$_2$ and Cu NP's.

FESEM images of CMT(3)-350 shown in Fig. 3, revealed the formation of amorphous composite where

surface incorporated copper oxide is visible as the dark shades. ICP elemental analysis (Table S5) and

FESEM-energy dispersive X-ray (FESEM-EDXS) analysis (Fig. 3d, Table S4) confirmed that the Cu content in the CMT(3)-350 photocatalyst was near identical to the nominal loading of 3 wt% Cu. The elemental mapping image in Fig. 3b and 3c further revealed the distribution of the copper and titanium elements in the CMT(3)-350 where copper species is uniformly dispersed onto semiconductor surface.
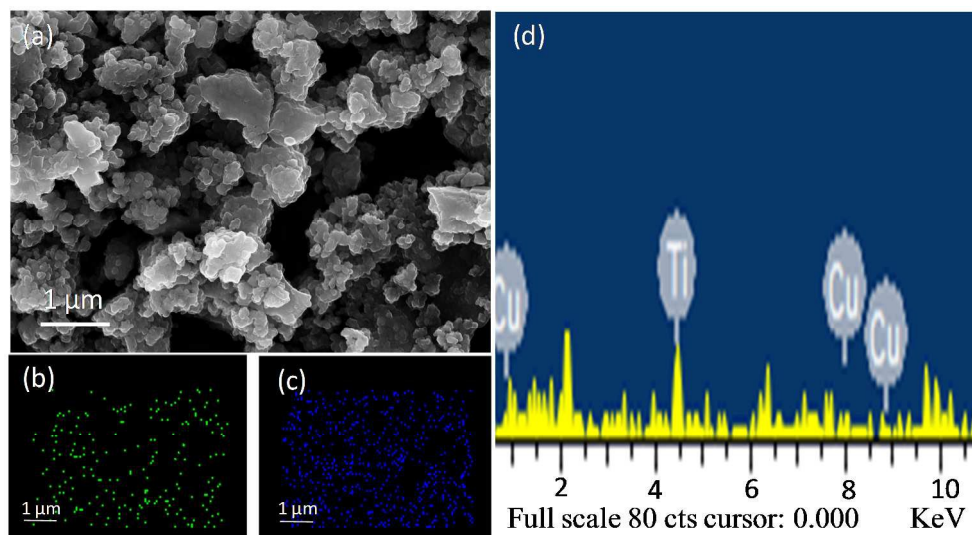
Fig. 3 (a) FESEM image, (b) EDXS pattern, (c) copper mapping, and (d) titanium mapping in CMT(3)-350.

PXRD patterns of before and after irradiated photocatalysts were incorporated in Fig. 4. As shown in Fig. 4a an 4b, the before irradiated photocatalyst samples (CMT(3)-350 and CMT(3)-450) showed their characteristic diffraction peaks (2θ) at $25.21°$, $37.91°$, $48.31°$, $53.81°$ and $55.01°$ represent the corresponding indices of (101), (103), (200), (105) and (211) planes respectively for anatase phase. These peaks were retained in the after irradiated CMT(3)-350 and CMT(3)-450 samples, as shown Fig. 4c and 4d respectively. A very low intense peak appeared at $38°$ in XRD pattern of irradiated photocatalysts, this may attributed to the presence of rutile phase in the catalyst (Fig. 4c and d). Besides, the intercalation of the copper species can be ruled out as no new peak was detected in the XRD pattern. We have confirmed the presence of Cu NP and CuO on TiO_2 surface by recording the XRD pattern of Cu/CuO@TiO_2 nanocomposite at reasonably higher Cu concentration (30 wt%). As shown in Fig. 4(ii) diffraction peaks at $35.5°$ and $38.7°$ attributed to (002) and (111) plane of CuO respectively, whereas a low intense peak at $43°$ confirmed the Cu^0 crystalline structure having (111) plane as exposed facet. The

characteristic Cu-MOF peak of XRD can be shown in the Fig. S3†. It indicates the presence of solvent coordinated Cu-BDC ([Cu(tpa).(dmf)]). The low intense peaks at 8º and 8.5º may due to the [Cu(tpa)].[8]
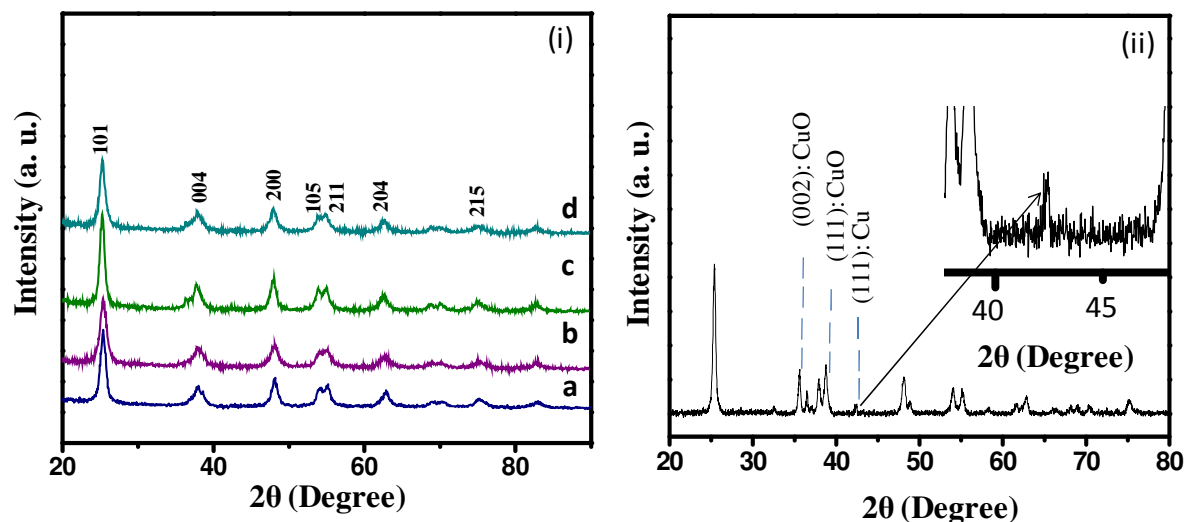
Fig. 4 XRD pattern of before irradiate catalysts (a) CMT(3)-350, (b) CMT(3)- 450 and after irradiated catalysts (c) CMT(3)-350, (d) CMT(3)-450 (ii) XRD pattern of Cu/CuO@TiO$_2$ at 30 wt% Cu loading.

Specific surface area of the nanocomposite has a direct correlation with surface active sites which turn out to be a controlling factor in photocatalytic activity.[11] The specific surface area was calculated from the linear region of the BET plot (Fig. 5 and Table 1) ranging from $P/P_0 = 0.1$ to 0.4. With 3 wt% Cu loading the BET surface area of the Cu/CuO@TiO$_2$ nanocomposites calcined at 350 °C and 450 °C are 45.3 and 41.9 m^{2}g^{-1} respectively, which is little higher in comparison to pristine TiO$_2$ with surface area of 38 m^{2}g^{-1} (Fig. 5). A hysteresis loop in the type-IV isotherm adsorption-desorption isotherm was observed at higher pressures indicating the presence of mesopores.[12]
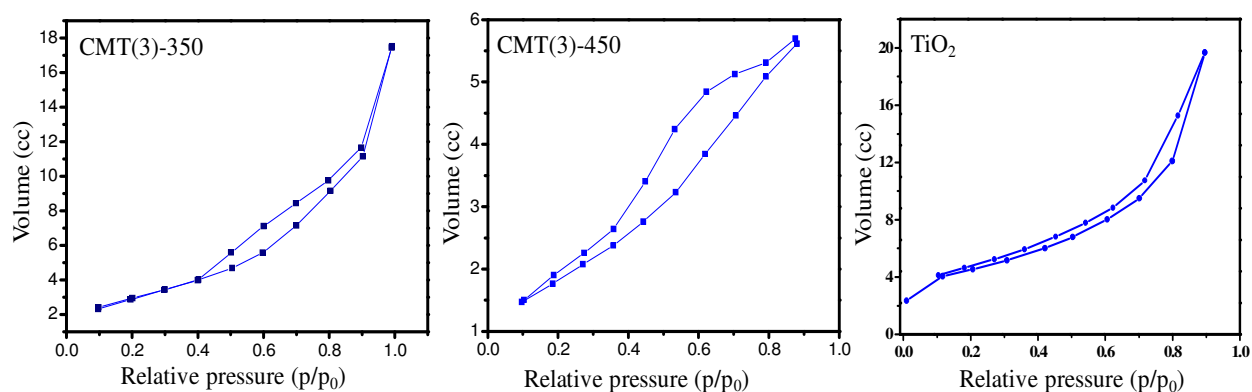
Fig. 5 BET isotherm of (a) CMT(3)-350, CMT(3)-450 nanocomposite and TiO₂.

Moreover, the as-observed from the pore size distribution curve (Fig. S4†) average Barrett–Joyner–Halenda (BJH) pore diameter for CMT(3)-350 and CMT(3)-450 are 3.51 nm and 3.84 nm respectively, indicates the mesoporous nature of the as-prepared nanocomposites according to the IUPAC convention.

Table 1. Surface area, pore radius, and pore volume of CMT(3)-350 and CMT(3)-450 measured by BET surface analyzer.

Catalyst	Surface area (m^2/g)	Pore diameter (nm)	Total pore volume(cc/g)
CMT(3)-350	45.3	3.51	0.25
CMT(3)-450	41.9	3.84	0.19

It was also found that the total pore volume of the photocatalyst decreased an amount of 0.06 cc/g, which may attributes to the lowering of surface porosity due to increase in calcination temperature. These change in surface properties could taking down the photoactivity of CMT(3)-450 in comparison to CMT(3)-350.

TGA of hydroxo titanium (IV) coated Cu-BDC (Cu-BDC@Ti(OH)$_n$)was carried out to sketch out the composition weight loss (Fig. S5†). It was found that the major weight loss happened between 60 to 210 ℃ which included the removal of cluster water molecule from hydroxo cluster and one DMF solvent molecule per monomer of Cu-BDC. In the second step, the weight loss was due to the conversion of hydroxo form to TiO₂. A further weight loss occurred at high temperature between 300-400 ℃, where the organic counterpart lost from the MOF architecture that left highly dispersed Cu and CuO on TiO₂ surface.

Optical properties were investigated for CMT(3)-350 and CMT(3)-450 composites by using DRS and the results were depicted in Fig. 6. The spectrum of pure TiO₂ showed band gap absorption near 370 nm, which is typical for the anatase TiO₂ nanoparticles. The as-prepared hybrid composites showed broad visible light absorption up to 600 nm, which was retained after light irradiation during photocatalysis. This indeed attributes to the significant stability and recyclability of catalyst for H₂ generation under the

long term solar irradiation. A broad absorption over the range of 600 – 800 nm is assigned to the pure d-d transition of Cu (II),[13] which is observed before and after photocatalytic experiment. Therefore, a very prudent contextual analysis supported that nano Cu crystallites and CuO flanked irregularly on the TiO_2 surface, formed Schottky (metal-semiconductor) barriers and small size heterojunction, which enhance charge separation and increase the quantum efficiency in solar harvesting materials.[10,14]
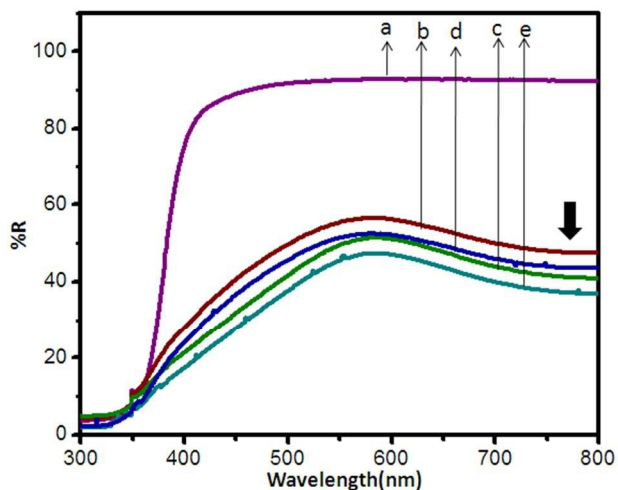
Fig. 6 UV-vis DRS of (a) TiO_2, (b) CMT(3)-350 (before irradiation), (c) CMT(3)-450 (before irradiation), (d) CMT(3)-350 (after irradiation) and (e) CMT(3)-450 (after irradiation).

The surface and sub-surface components with their chemical states of $Cu/CuO@TiO_2$ heterocomposite of CMT(3)-350 were examined by XPS analysis, and the results are shown in Fig 7. All binding energies were calibrated using the contaminant carbon (C 1s = 283.3eV) as the reference. Fig 7a showed the full range scan survey spectra for representative $Cu/CuO@TiO_2$ heterocomposite CMT(3)-350. In accordance with the previous report, the characteristic peaks of Ti $2p_{3/2}$ and $2p_{1/2}$ for TiO_2 based composites appeared at the binding energy (BE) of 458.9 eV and 464.5 eV respectively (Fig. 7b).[15] Subsequently, O 1s (Fig. 7c) and Cu $2p_{3/2}$ core level peaks (Fig. 7d) appeared at 530 eV and 931.9 eV respectively. The high BE observed for main line along with satellite features of around 945 eV demonstrates the oxidation state of copper remains to be in Cu^{2+} which was further supported by the DRS study. No spectral feature was observed at around 932.5 eV for metallic Cu,[16] is likely due to its small percentage on the surface. Moreover, we did not observed any characteristics for Cu^+ species, which appears at 932.3 eV, though it

is really difficult to distinguish those ions because of their marginal difference in binding energy values.
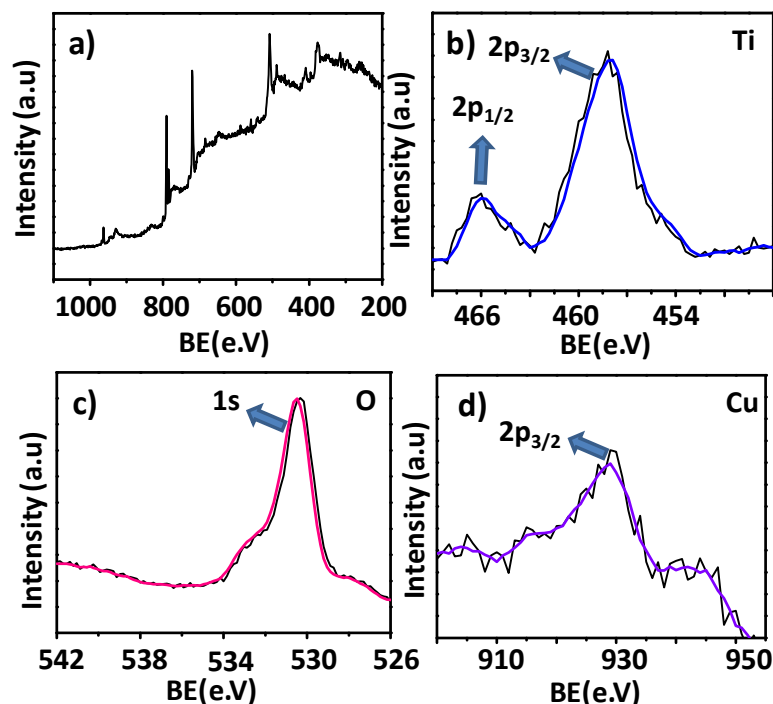
Fig. 7 XPS survey of CMT(3)-350 catalyst (before irradiation), (a) full scan survey, (b) Ti 2p, (c) O 1s and d) Cu 2p core level spectra.

Photocatalytic H$_2$ generation

Photocatalytic H$_2$ evolution studies were performed over various Cu/CuO@TiO$_2$ catalysts in presence of scavengers under solar irradiation. The apparent quantum efficiency (AQE) was estimated by the reported equation.[4b] The individual component of the as-prepared composites are virtually inactive for H$_2$ production performance. We did not observe any H$_2$ production yield, when 15% aqueous CH$_3$OH solution was irradiated in presence of 25 mg CuO, whereas pure TiO$_2$ produced only 12.5 µmol of H$_2$ after 6 h under similar experimental condition. The significance of the synthesis methodology was clearly illuminated from the high AQE value in terms of H$_2$ production for as-prepared photocatalysts than that of Cu doped TiO$_2$ and CuO loaded TiO$_2$ (Table 2), where Cu doped TiO$_2$ and CuO loaded TiO$_2$ were prepared using reported method.[17]

Table 2. Comparison of the photocatalytic H_2 production results of present study with the other copper based photocatalytic system.

Photocatalyst	Preparation method	[b]Rate (mmol/g/h)	AQE (%)
[a]CMT(0.5)-350	MOF templated	286	10.5
[a]CMT(0.5)-450	MOF templated	270	9.88
[a]Cu doped TiO_2	NH_3 evaporation-induced synthetic method	124	3.5
[a]CuO loaded TiO_2	Impregnation method	65	2.34
[18]Cu/TiO_2	Ion exchange	3.12	-
[9]Cu/TiO_2/graphene	Hydrothermal followed by photo-irradiation	100	-
[15]Cu_2O/TiO_2	Impregnation method	200.6	-

[a]Present work. [b]Rate was calculated with same unit in order to compare the photoactivity.

The H_2 generation efficiency of different wt% Cu loaded TiO_2 photocatalysts were investigated in aqueous solution containing CH_3OH as SED and the results were depicted in Fig. S6a**,** S6b and Table S1†. It is worth noting that the 0.5 wt% of Cu loading was found to be optimal amount for best catalytic performance. A significant decrease in H_2 yield was observed above 0.5 wt% loading, and is more prominent from 3 to 5 wt% Cu loading. Hydrogen production yield was not greatly influenced on varying the Cu content from 0.3-1 wt% (Fig. S6a and S6b†). As an added benefit, for screening other operational parameter, 3 wt% of Cu loading was chosen in order to maintain a better clarity with the photophysical studies. The balance between increase in trapping sites and fewer trapped carriers depends on the existence of optimal Cu concentration (0.5 wt% Cu) in the photocatalysts. This leads to longer life time for interfacial charge transfer.[19] However, the cocatalyst cluster at a higher concentration, work as a recombination center and recombination between electron and hole increases exponentially with the increase in loading concentration.[19] As a matter of fact, the average distance between the trapping site decreases with the increase in number of cluster confined within the particle. According to Xu and Sun, active sites of the photocatalyst for hydrogen generation was probably located at the interfacial position of

catalyst surface rather than on the isolated co-catalyst or TiO_2.[20] It is important to note that the effect of the calcination temperature on the H_2 generation plays an important role as it controls the chemical status of Cu and the phase morphology of TiO_2. It is found that photocatalysts calcined at 350 ℃ showed comparatively greater activity than the catalysts calcined at 450 ℃, which might be due to partial loss of surface active sites at high temperature calcination. The dosage of photocatalyst is a vital parameter in all photocatalytic reactions. It was observed that initially the photocatalytic activity increased with increase in the photocatalyst amount up to 25 mg and, later on, the activity decreased with increase in amount. At a lower dose, the number of active sites is also lower, resulting into lower hydrogen evolution. In particular, 25 mg of CMT(3)-350 and CMT(3)-450 photocatalyst has reached 8% and 7.74% AQE after 6 h irradiation (Fig. 8 and Fig. S6c, S6d and Table S2†). A further increase in the amount of catalyst, reduces the penetration depth of the incident light which may increase the possibility of losing scattered light to the exterior and reduce the hydrogen production yield.[21]
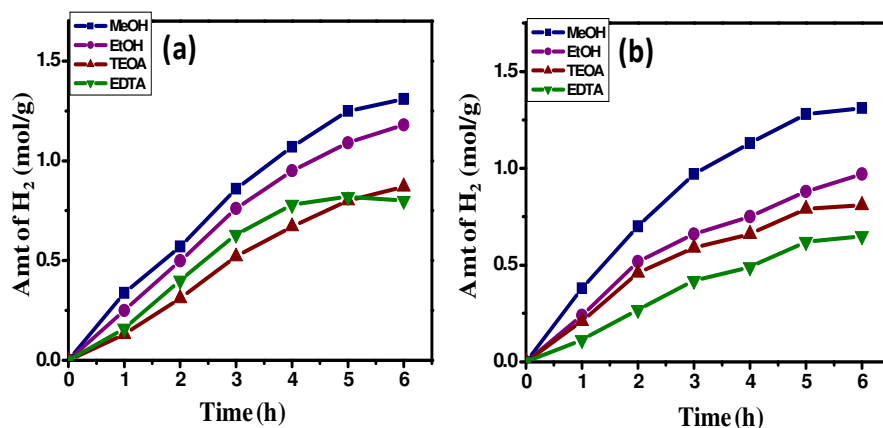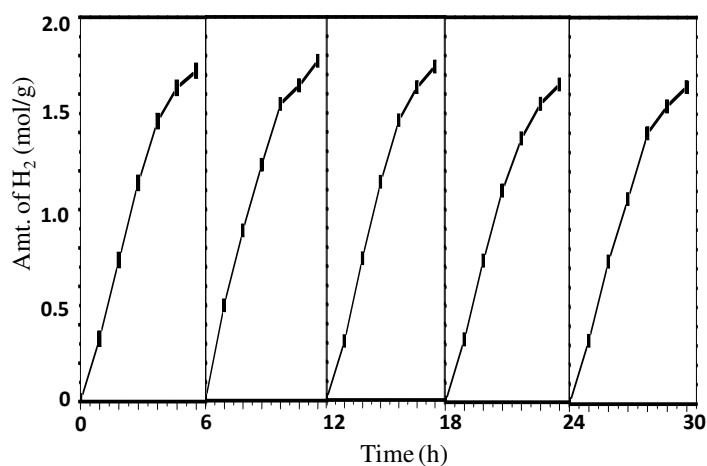

Fig. 8 Time course of photocatalytic H_2 evolution over 25 mg of (a) CMT(3)-350 and (b) CMT(3)-450 in different aqueous SED (15% v/v) system, under UV-Visible light irradiation.

The photocatalytic systems studied under a wide range of SED's. Since, SED's or hole scavengers can react with the valence band holes and prevent the recombination reaction. So, SED's are considered as effective means of increasing the photocatalytic activity. Photoactivity of CMT(3)-350 and CMT(3)-450 was tested under four different SED's namely CH_3OH, C_2H_5OH, EDTA and triethanolamine (TEOA) under identical condition, shown in Fig. 8 and Table S3†. Among all the SED used, maximum H_2 evolution yield was obtained with CH_3OH. While moving to the photocatalytic results, significant hydrogen

production yield was observed with 1.31 and 1.27 mol/g for CMT(3)-350 and CMT(3)-450 respectively in aqueous solution containing CH_3OH as SED.

Photocatalytic recyclability was tested using 0.5 wt% Cu loaded CMT(0.5)-350 photocatalysts in presence of aqueous MeOH solution (Fig. 9). The result shows that the hydrogen evolution amount of CMT(0.5)-350 photocatalyst decreased slightly after 3rd cycle. This is probably caused by disruption of the interactions between the co-catalysts and the semiconductor surfaces after extended periods of irradiation and stirring. It is worth mentioning here that, morphological and optical properties of the used catalyst clearly show the retentivity by the catalyst. However, we have noticed during irradiation, the colour of the photocatalyst little blackish, which may due to trapped electrons in the CuO cluster and the chance of formation of more Cu nanoparticle in the reaction mixture.[10] However, when the photocatalyst was taken out from reactor (Fig. S7†) filtered and washed for further use, it turned into original colour.

Fig. 9 Time courses for recyclability of photocatalytic H_2 evolution: 25 mg of CMT(0.5)-350 suspended in a 15% v/v of aqueous MeOH solution under UV-visible light. Arrows indicates evacuation.

The enhanced photoactivity of the as-prepared composite was further supported by measuring the photocurrent using LSV in the dark and under visible light irradiation, shown in Fig. 10(a). In this experiment Cu doped TiO_2 and CuO loaded TiO_2 was tested as control which was prepared by reported method.[17] Generally, a high photocurrent indicates that the sample has a strong ability to generate and transfer the photoexcited charge carriers during the course of photo-irradiation.[22] Cu/CuO@TiO_2 showed

a higher photocurrent in comparison to other catalyst under the same evaluation condition, suggesting that Cu/CuO@TiO$_2$ exhibits a stronger ability for e$^-$/h$^+$ pair separation than that of Cu doped TiO$_2$ and CuO loaded TiO$_2$. Moreover, EIS was performed on a Cu/CuO@TiO$_2$ nanocomposite to examine the charge transfer resistance and separation efficiency between the photogenerated electrons and holes Fig. 10(b) shows typical EIS Nyquist plots of the CMT(3)-350 photocatalysts in the dark and under UV-vis light irradiation. The arc radius of the EI (electrochemical impedance) spectra indicates the interface layer resistance arising at the surface of the electrode. We observed a lower resistance in the photocatalyst under light irradiation, as confirmed by the smaller arc radius of EI spectra. This is attributable to photo-induced charge transfer from TiO$_2$ to CuO and Cu NP, which accelerated the electron-hole separation during the course of reaction.
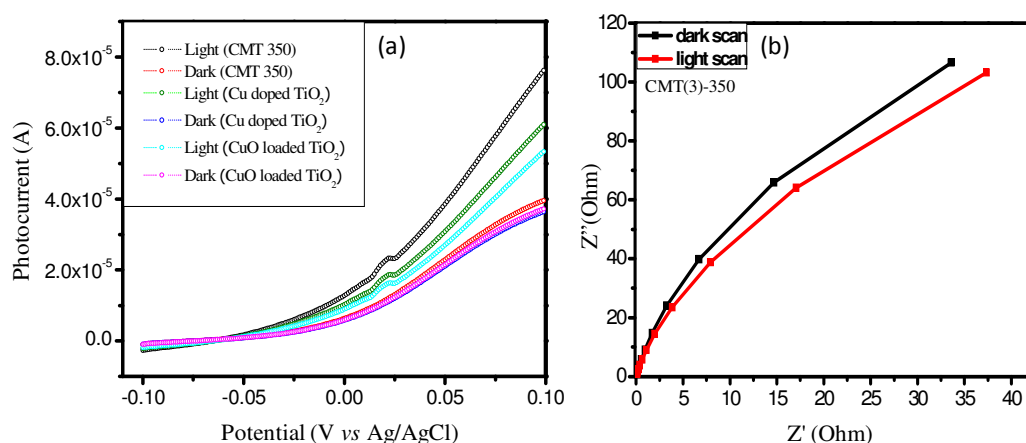

Fig. 10 LSV of CMT(3)-350 in light and dark condition. (b) Nyquist plots of electrochemical impedance spectra in dark and light condition.

Based on the structural analysis, it can be unambiguously identified that, the as-synthesized photocatalyst contains CuO and Cu^0 species, which is highly distributed with an irregular pattern on TiO$_2$ semiconducting surface. It was observed that platinized TiO$_2$ is showed poor photoactivity in comparison to as-prepared Cu/CuO@TiO$_2$ hybrid system. Indeed, based on experimental observations, we have rationalized the plausible mechanistic insight for enhanced photoactivity of Cu/CuO@TiO$_2$ photocatalyst, shown in Fig 11.
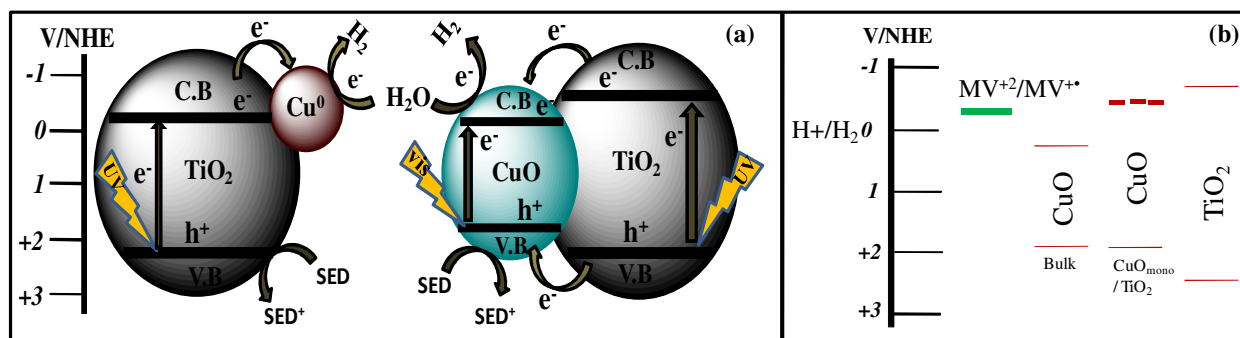
Fig. 11 (a) Possible mechanism of utilization of charge carriers in photocatalytic H_2 generation over Cu/CuO@TiO$_2$ and **(b)** band alignment of different photocatalysts.

It is suggested that copper species with lower concentration generally adsorbed as a sub-monolayer on host semiconducting surface. As a consequence, the Fermi level for such adsorbed species aligned at positive potential with respect to the conduction band (CB) of TiO$_2$. Moreover, during the course of irradiation, electrons in the VB of CuO can also be excited to reach the CB. The excess electron accumulation in CB of CuO leads to shifting of CB potential towards more a negative region, lower than the redox potential of H^+/H_2.[23] In this concurrence, the shifting of CuO CB edge towards more negative potential was confirmed by monitoring the electron transfer process using methyl viologen (MV^{+2}) as probe under visible light irradiation (> 400 nm). MV^{2+} is a perfect system in this regard because it possesses pH independent reduction potential of E^0 ($MV^{2+}/MV^{+\bullet}$) = −0.446 V, vs NHE.[24]
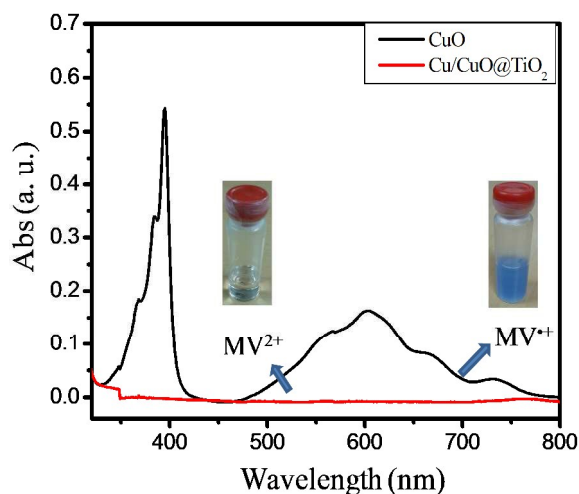
Fig. 12 (a) Absorption spectra of 2 mg of photocatalyst in deaerated 4 ml of 100 μM MV^{2+} before (red) and after (black) irradiation (λ > 400 nm). A digital photograph shows the colour of MV^{2+} and photo-reduced $MV^{+\bullet}$.

As shown is Fig. 12, no colour change was observed when aqueous MV^{2+} solution was irradiated in presence of pure CuO having CB potential of 4.9 V *vs* Absolute vacuum Scale Whereas, a blue colour solution formed (λ_{max} = 605 nm) in presence of Cu/CuO@TiO$_2$ composite, confirmed the successful conversion of MV^{+2} to $MV^{+\bullet}$. Moreover, this is also attributed that electrons in the CB of CuO can also be photoexcited under visible light irradiation. Therefore, H$_2$ evolution occurred at the H$_2$O/CuO interface with easy flow of photoexcited electrons from the CB of TiO$_2$ to the CB of CuO, while the photoexcited holes in the valence band (VB) of TiO$_2$ transfer to the VB of CuO. Notably, the small size heterojunction may play a pivotal role in this phenomenon. On the other hand, Fermi level created by the Cu NP's is –ve with respect to H$^+$/H$_2$ redox potential but +ve with respect to CB potential of TiO$_2$ which synergize the H$_2$ production efficiency by accelerating the interfacial charge transfer and suppressing charge recombination. [25]

Conclusions

The impulsion for the work demonstrated herein was to construct Cu/CuO@TiO$_2$ hybrid system, which is still elusive despite the surplus of reports on metal oxide and/or metal NP based photocatalysts. Accordingly, we have successfully constructed and characterized MOF-derived Cu/CuO@TiO$_2$ system where copper species are dispersively and irregularly adsorbed on the anatase TiO$_2$ surface. We have further reinforce our idea that proper utilization of surface engineering can lead to better attachment of TiO$_2$ precursors at the surface of parents MOFs, and ultimately yield to better catalyst. At optimized Cu loading, we observed the maximum photocatalytic hydrogen evolution rate of 286 mmolg^{-1}h^{-1}, which is significantly higher than many earth-abundant metal oxide based photocatalysts reported to date. The formation of small size heterojunction between CuO and TiO$_2$ and the cocatalytic role of Cu NP should be attributable to synergistic interfacial charge transfer and efficient electron-hole separation in the photocatalytic reaction. Moreover, the as-prepared photocatalyst exhibited stable H$_2$ evolution activity for several reuse cycles over 30 h. This work may open up a new insight for the fabrication of MOF-templated heterocomposite consisting of earth abundant metal oxide clusters to improve photocatalytic

activity with desirable synergistic properties.

Notes and references

1. A. Fujishima and K. Honda, *Nature*, 1972, **238**, 37-38.
2. (a) S. J. A. Moniz, S. A. Shevlin, D. J. Martin, Z. X. Guo and J. Tang, *Energy Environ. Sci.*, 2015, **8**, 731-759. (b) P. V. Kamat, *J. Phys. Chem. Lett.*, 2012, **3**, 663–672. (c) S. K. Dutta, S. K. Mehetor and N. Pradhan, *J. Phys. Chem. Lett.*, 2015, **6***, 936–944.
3. Y. Ma, X. Wang, Y. Jia, X. Chen, H. Han and C. Li, *Chem. Rev*. 2014, **114**, 9987–10043. (b) S. Mukhopadhyay, I. Mondal, U. Pal and P. S. Devi, *Phys. Chem. Chem. Phys.*, 2015, **17**, 20407-20415.(c) A. Kudo, Y. Miseki, *Chem. Soc. Rev*., 2009, **38**, 253-278.
4. (a) Z. Wang, Y. Liu, D. J. Martin, W. Wang, J. Tang and W. Huang. *Phys. Chem. Chem. Phys.*, 2013, **15**, 14956-14960. (b) S. Bala, I. Mondal, A. Goswami, U. Pal and R. Mondal, *J. Mater. Chem. A*, 2015, **3**, 20288–20296. (c) J. Lin, J. Shen, R. Wang, J. Cui, W. Zhou, P. Hu, D. Liu, H. Liu, J. Wang, R. I. Boughton and Y. Yue, *J. Mater. Chem.*, 2011, **21**, 5106–5113.
5. (a) Y. J. L. Qi and M. Jaroniec, *J. Phys. Chem C,* 2010, **114**, 13118–13125. (b) M. Murdoch, G. I. N. Waterhouse, M. A. Nadeem, J. B. Metson, M. A. Keane, R. F. Howe, J. Llorca and H. Idriss, *Nature Chem.*, 2011, **3**, 489-492.
6. (a) C. Li, T. Chen, W. Xu, X. Lou, L. Pan, Q. Chen and B. Hu, *J. Mater. Chem. A*, 2015, **3**, 5585–5591. (b) W. Wang and D. Yuan, *Sci. Rep.*, 2014, **4(5711)**, 1–7. (c) Y. P. Yuan, Y. J. Zhu, X. Jiang, J. D. Xiao, Y. F. Zhang and L. G. Qiu, *Appl. Catal., B*, 2014, **144**, 863–869. (d) K. E. deKrafft, C. Wang and W. Lin, *Adv. Mater.*, 2012, **24**, 2014–2018.
7. Y. Han, P. Qi, S. Li, X. Feng, J. Zhou, H. Li, S. Su, X. Li and B. Wang, *Chem. Commun*., 2014, **50**, 8057–8060.
8. C. G. Carson, K. Hardcastle, J. Schwartz, X. Liu, C. Hoffmann, R. A. Gerhardt, R. Tannenbaum, *Eur. J. Inorg. Chem.*, 2009, **2009**, 2338-2343.

9. X-J. Lv, S-X. Zhou, C. Zhang, H-X. Chang, Y. Chen, W-F. Fu, *J. Mater.Chem.,* 2012, **22**, 18542-18549.

10. G. D. Moon, J. B. Joo, I. Lee, Y. Yin, *Nanoscale*, 2014, **6**, 12002-12008.

11. T. Bak, W. Li, J. Nowotny, A. J. Atanacio and J. Davis, *J. Phys. Chem. A*, 2015, **119***,* 9465–9473.

12. A. S. Hall, A. Kondo, K. Maeda and T. E. Mallouk, *J. Am. Chem. Soc*., 2013, **135**, 16276–16279.

13. H. Yu, H. Irie and K. Hashimoto, *J. Am. Chem. Soc*., 2010, **132**, 6898–6899.

14. L. Liu, Z. Ji, W. Zou, X. Gu, Y. Deng, F. Gao, C. Tang and L. Dong, *ACS Catal*., 2013, **3**, 2052–2061.

15. K. Lalitha, G. Sadanandam, V. D. Kumari, M. Subrahmanyam, B. Sreedhar and N. Y. Hebalkar, *J. Phys. Chem. C,* 2010, **114**, 22181–22189.

16. S. Velu, K. Suzuki, M. Vijayaraj, S. Barman and C. S. Gopinath, *Appl. Catal. B*, 2005, **55**, 287-299.

17. (a) Y. Li, B. Tan and Y. Wu, *Chem. Matter*., 2008, **20**, 567–576. (b) J. Bandara, C. P. K. Udawatta and C. S. K. Rajapakse, *Photochem. Photobiol. Sci*., 2005, **4**, 857-861.

18. H. Tian, X. L. Zhang, J. Scott, C. Ng and R. Amal, *J. Mater. Chem. A*, 2014, **2**, 6432–6438.

19. W. Y. Choi, A. Termin and M. R. Hoffmann, *J. Phys. Chem.,* 1994, **98**, 13669–13679.

20. S. Xu and D. D. Sun, *Int. J. Hydrogen Energy*, 2009, **34**, 6096–6104.

21. P. Maruthamuthu, M. Ashokkumar, K. Gurunathan, E. Subramania and M. V. C. Sastri, *Int. J. Hydrogen Energy,* 1989, **14**, 525-528.

22. (a) X. Bai, L. Wang, R. Zong, Y. Lv, Y. Sun and Y. Zhu, *Langmuir*, 2013, **29**, 3097–3105. (b) J. Gan, X. Lu, J. Wu, S. Xie, T. Zhai, M. Yu, Z. Zhang, Y. Mao, S. C. Wang, Y. Shen and Y. Tong, *Sci. Rep.*, 2013, **3**, 1021–1028.

23. F. Teng, M. Chen, N. Li, X. Hua, K. Wang and T. Xu, *ChemCatChem*, 2014, **6**, 842 – 847.

24. S. Krishnamurthy and P. V. Kamat, *J. Phys. Chem. C,* 2013, **117**, 571–577.

25. M. T. Greiner, M. G. Helander, W-M. Tang, Z-B. Wang, J. Qui, Z-H. Lu, *Nature Mater.,* 2012, **11**, 76-81.

‡ U. Pal, I. Mondal, Photocatalyst containing earth abundant materials and hydrogen production thereof, Patent application no. 2337/DEL/2015*,* Innovation Protection Unit (IPU), CSIR, India.

TOC